Multispectral time-resolved energy-momentum microscopy using high-harmonic extreme ultraviolet radiation

Michael Heber,[1, a)] Nils Wind,[2, 3, a)] Dmytro Kutnyakhov,[1, b)] Federico Pressacco,[1] and Kai Rossnagel[3, 4]
[1)] *Deutsches Elektronen-Synchrotron DESY, Germany*
[2)] *Department of Physics and Centre for Free-Electron Laser Science CFEL, University of Hamburg, Germany*
[3)] *Ruprecht-Haensel-Labor RHL, Deutsches Elektronen-Synchrotron DESY, Germany*
[4)] *Institut für Experimentelle und Angewandte Physik, Christian-Albrechts-Universität zu Kiel, Germany*

A 790-nm-driven high-harmonic generation source with a repetition rate of 6 kHz is combined with a plane-grating monochromator and a high-detection-efficiency photoelectron time-of-flight momentum microscope to enable time- and momentum-resolved photoemission spectroscopy over a spectral range of 23.6–45.5 eV with sub-100-fs time resolution. Three-dimensional (3D) Fermi surface mapping is demonstrated on graphene-covered Ir(111) with energy and momentum resolutions of $\lesssim$100 meV and $\lesssim$0.1 Å^{-1}, respectively. The table-top experiment sets the stage for measuring the k_z-dependent ultrafast dynamics of 3D electronic structure, including band structure, Fermi surface, and carrier dynamics in 3D materials as well as 3D orbital dynamics in molecular layers.

I. INTRODUCTION

Angle-resolved photoemission spectroscopy (ARPES) is the standard method to determine how electrons behave at surfaces of solid materials.[1–4] Monochromatic photons having ultraviolet (UV) energies or higher eject electrons from a material's surface, and the photocurrent is measured as a function of electron kinetic energy, emission direction, and photon energy. Direction is encoded in two emission angles or, equivalently, in the two components of the surface-parallel momentum (k_x, k_y). Since the four measurement parameters can be straightforwardly related to the energy relative to the Fermi level ($E - E_F$) and three-dimensional (3D) momentum (k_x, k_y, k_z) of the electrons inside the material before photoexcitation,[5] the measured intensity distributions readily provide multidimensional images of the electronic structure in portions of four-dimensional (4D) energy-momentum space.[6] Band structures and Fermi surfaces, but also momentum-dependent band renormalization and lifetime effects, can thus be accessed directly.[7–10] Another intriguing application is orbital tomography, which can provide reconstructed real-space tomograms of molecular orbitals on solid surfaces.[11,12] Depending on whether emission angles or surface-parallel momentum components are imaged onto the detector,[13–15] the technique is referred to as ARPES or momentum microscopy, respectively.

In this energy-momentum imaging, the photon energy is an important parameter in at least three different ways. First, the photon energy determines the maximum detectable electron kinetic energy and 3D momentum, and thus the volume of the probed portion in energy-momentum space.[16] Second, the photon energy needs to be scanned, if full 4D energy-momentum imaging, which specifically includes control of the surface-perpendicular momentum component k_z, is to be performed.[6,10,17,18] And third, tunability in the photon energy can also be useful to enhance the contrast of specific features in ARPES data by exploiting excitation resonances, escape-depth variation, or matrix-element effects.[19,20]

In principle, the same relevance of the probing photon energy and its tunability also applies to time-resolved ARPES (trARPES) or time-resolved momentum microscopy,[21,22] in which time, or more precisely the time delay (t_D) between femtosecond-scale pump and probe pulses, is added as a fifth measurement parameter. Over the past fifteen years, trARPES has evolved into a powerful ARPES modality providing direct dynamical information on electronic structure at the fundamental time scales of electronic and atomic motion, particularly on photoinduced transient changes of electronic states and their population.[23–32] trARPES is now routinely performed using table-top laser sources based on fourth and higher harmonic generation (HHG) in solids[33,34] and gases[35–50], respectively, as well as using free-electron lasers (FELs) based on the self-amplification of spontaneous emission (SASE) of free electrons in undulators.[21] The corresponding probe photon energies in trARPES range from the far UV to soft x-rays where a sweet spot currently is the intermediate extreme ultraviolet (XUV) regime.

In the XUV, HHG-based trARPES can optionally provide high time, energy, and momentum resolution in conjunction with kHz-to-MHz repetition rates and a sufficiently wide detection window of the surface-parallel momentum (k_x, k_y) to fully cover typical Brillouin-zone (BZ) dimensions.[35–50] Moreover, HHG sources combined with monochromators enable multispectral measurements as they can deliver a useable, discretely tunable photon-energy range of ≈8–40 eV.[35,36,40,43,44,46] However, this multispectral capability has so far rarely been exploited in trARPES experiments, and recently several setups for HHG-based trARPES have even been optimized for operation at one specific photon energy only.[37,41,47,48] Here, contrary to this trend, we present the combination of a tunable, monochromatized, kHz-repetition-rate HHG source with a wide-momentum-acceptance time-of-flight (ToF) momentum microscope for efficient 4D energy-momentum mapping of ultrafast electronic structure dynamics. The overall system performance is demonstrated on bare

[a)] These authors contributed equally to this work.
[b)] Electronic mail: dmytro.kutnyakhov@desy.de

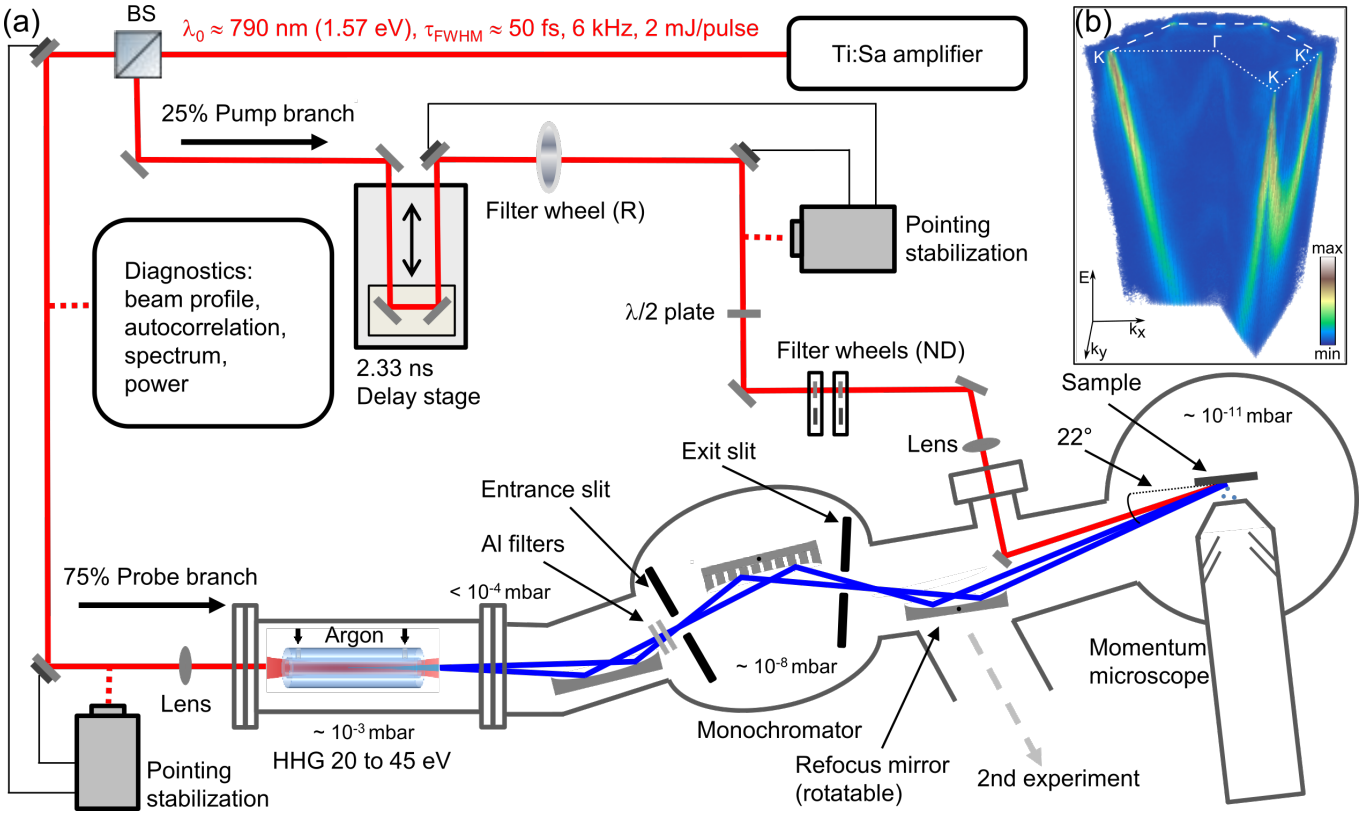

FIG. 1. (a) Schematic layout of the experimental setup for XUV multispectral time-resolved momentum microscopy, including the laser system, optics, and diagnostics, the Ar-filled capillary for HHG, the plane-grating monochromator, and the ToF momentum microscope for photoelectron detection. For details, see text. BS: beam splitter, R: reflective, ND: neutral density. (b) Exemplary 3D momentum microscopy data set representing photoemission intensity as a function of energy E and surface-parallel momentum (k_x, k_y). Data was measured with the 27$^{\text{th}}$ harmonic (42.2 eV) from graphene/Ir(111) and symmetrized by three-fold rotation. The hexagonal Brillouin zone of graphene is indicated.

and graphene-covered Ir(111).

II. EXPERIMENTAL SETUP

Our multispectral-HHG trARPES setup, as schematically illustrated in Fig. 1, measures a 5D photoemission data hypercube $I(E,k_x,k_y;k_z,t_\mathrm{D})$. The laser system provides the tuning of k_z and t_D, via adjustability of the probe photon energy and pump–probe delay, respectively, and the ToF momentum microscope provides the basic parallel 3D measurement of $I(E,k_x,k_y)$.

A. Multispectral photon source

The schematic layout of the laser system is shown in Fig. 1(a). A Ti:Sapphire laser amplifier (Wyvern 1000, KM-Labs), operated an output power of 12 W and at a repetition rate of 6 kHz, delivers laser pulses at a center wavelength of ≈790 nm, pulse duration of ≈50 fs (FWHM, full width at half maximum), and pulse energy of ≈2 mJ. A quarter of the amplifier output is coupled into the pump branch, propagated through a delay stage, and focused onto the sample in the ultrahigh vacuum (UHV) photoemission chamber. The spot size of the pump beam on the sample is typically about $(100\times400)\,\mu\mathrm{m}^2$. The available pump-pulse energy of 500 μJ can be used for frequency conversion or attenuated to the mid-nJ to low-μJ level for 790-nm excitation of the sample below the space-charge limit.

The remaining 75% of the amplifier output are coupled into the probe branch and focused into an Ar-filled waveguide capillary (XUUS, KMLabs), where higher harmonics in the XUV are generated. During operation, the Ar pressure inside the capillary is ≈60 mbar, while the pressure outside stays below $\approx5\times10^{-3}$ mbar. A ZrO_2-coated toroidal mirror is used to focus the multispectral XUV light onto the entrance slit of the monochromator and to separate out much of the fundamental radiation. The remaining 790-nm light is blocked using few-100-nm thick Al filters. Differential pumping is used to maintain a 5-orders-of-magnitude pressure difference between the HHG source and the monochromator chamber. A rotatable Au-coated grating with 550 lines/mm images the entrance slit onto the exit slit with the selected higher harmonic light, and a second toroidal mirror focuses the selected and monochromatized XUV light onto the sample at an angle of 22° with respect to the surface. This mirror is rotatable and can alternatively direct the beam to a gas-phase experiment with com-

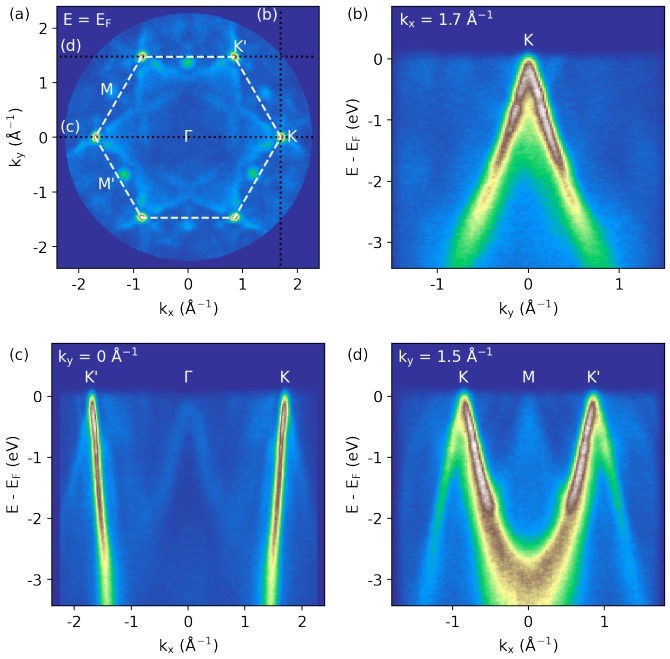

FIG. 2. Momentum microscopy data of graphene/Ir(111) recorded with a photon energy of 42.4 eV (27$^{\text{th}}$ harmonic). (a) k_x-versus-k_y Fermi surface map. The hexagonal Brillouin zone of graphene and its high-symmetry points are indicated. (b)–(d) E-versus-k band maps for different k lines as indicated by black dotted lines in (a).

bined ion- and electron-ToF spectroscopy.[51,52] Behind the refocusing mirror, the pump and probe beams propagate almost collinearly to the sample. At the sample, the XUV beam has a spot size of $(70 \times 800)\,\mu\text{m}^2$ and a flux of 3×10^8 photons/s in the brightest harmonics, which are usually the 23$^{\text{rd}}$ and 25$^{\text{th}}$ (see central panel of Fig. 4). The practically useable part of the harmonic spectrum contains all eight odd harmonics from the 15$^{\text{th}}$ to the 29$^{\text{th}}$ corresponding to a photon energy range of 23.6–45.5 eV. According to ray-tracing simulations, the temporal probe pulse broadening by the monochromator lies in the range of 50 fs, independent of the slit size. The spectral resolution is in the range of 120 meV, for slit sizes of 100 μm.

B. Electron momentum microscope

The ToF momentum microscope used in our laboratory-based setup is the same instrument used for FEL-based photoemission spectroscopy at the PG2 beamline of FLASH (DESY, Hamburg).[21] The high photoelectron detection efficiency of the instrument, which compensates for the moderate repetition rate of the photon pulses, results from a combination of three separate capabilities: (i) direct 2D momentum imaging with a field of view of $\pm 2.4\,\text{Å}^{-1}$ in both directions, (ii) simultaneous ToF energy recording in an energy window of 7 eV, and (iii) multi-hit detection of up to 3 electrons per pulse. The underlying principle of slit-less 3D photoelectron energy-momentum detection is implemented as follows:[15] The photocurrent emitted from the surface is imaged into an achromatic surface-parallel momentum image at the back-focal plane of the cathode objective lens; this hyperspectral image is subsequently magnified and high-pass-filtered by two lens systems, before it is spectrally dispersed in a field-free drift tube and finally captured on a delay-line detector (DLD). The 8-segment DLD (DLD6060-8s, Surface Concept) used in the current setup consists of two stacked 4-quadrant DLDs rotated by 45° with respect to each other. This novel detector provides improved multi-hit detection capability compared to a single 1- or 4-quandrant DLD, as well as improved resolution of hits occurring near segment boundaries. The length of the drift tube (800 mm) and temporal resolution of the detector (≈150 ps) translate into a nominal energy resolution of <40 meV for typical electron drift energies of 10–30 eV. The nominal momentum resolution is $<0.01\,\text{Å}^{-1}$, as given by the momentum field of view, active detector area (60 mm diameter), and the spatial resolution of the detector (≈80 μm).

The 3D energy-momentum measurement system, based on single-event detection, fills in the photoemission data cube $I(E,k_x,k_y)$ over energy and momentum intervals with a characteristic width of 7 eV and $4.8\,\text{Å}^{-1}$, respectively, at a repetition rate of 6 kHz. When delay-time scanning is added, the resulting size of a typical 4D data hypercube is ≈100 GB. An efficient data acquisition and data processing workflow is implemented using an open-source software package developed for high-throughput multidimensional photoemission spectroscopy experiments.[53] Figure 1(b) shows a 3D representation of an exemplary data set taken from graphene/Ir(111). Four different 2D cuts through this data set are shown in Fig. 2, including the Fermi surface map $I(E_\text{F},k_x,k_y)$ [Fig. 2(a)] and selected band maps $I(E,k_0,k_y)$ [Fig. 2(b)] and $I(E,k_x,k_0)$ [Figs. 2(c) and 2(d)] for different constant values of k_0 corresponding to lines passing through high-symmetry points of the graphene BZ, as indicated in Fig. 2(a). In these maps, the strongest signal stems from the π-band of graphene with its linear dispersion toward E_F and point-like Fermi surface at the K and K' points. The Ir 5d bands appear as much weaker features. Their interaction with the π-band, however, leads to distinct kinks in the π-band dispersion.[54] The presented data vividly illustrate the efficiency and completeness of the ToF momentum microscopy approach to photoelectron detection.

III. PERFORMANCE

We have characterized the performance of the experimental system by measuring the near-E_F electronic structure and the above-E_F carrier dynamics of graphene-covered and pristine Ir(111), respectively. Standard Ir(111) cleaning procedures and graphene growth recipes were applied.[55] Surface quality was checked by low-energy electron diffraction. All photoemission measurements were done at room temperature.

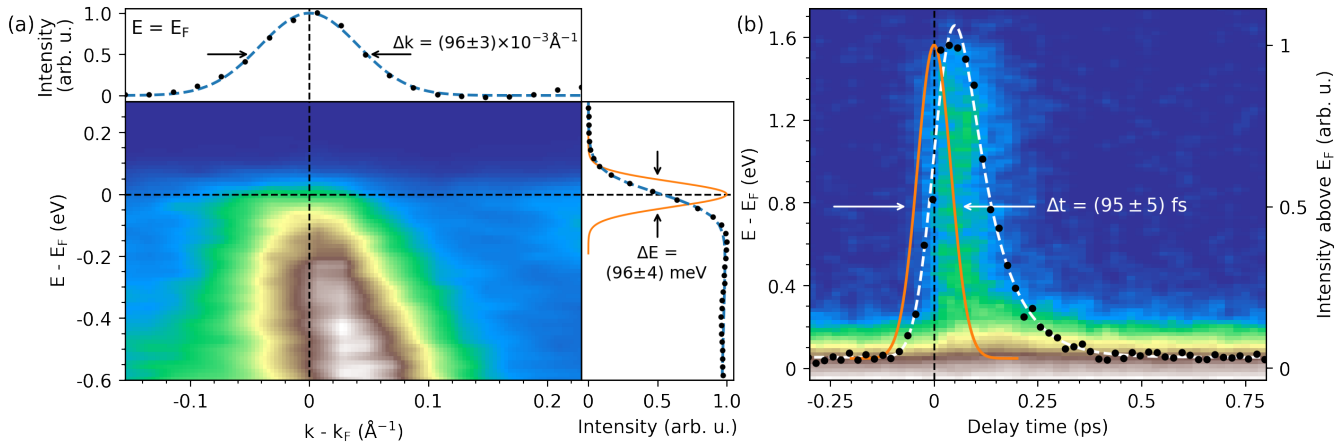

FIG. 3. (a) Energy-versus-momentum photoemission intensity map of graphene/Ir(111) recorded near the K point with a photon energy of 33.4 eV (21$^{\text{st}}$ harmonic). Top panel: Momentum distribution curve (black dots) at E_{F} plus fit (blue dashed line). Right panel: Energy distribution curve (black dots) representing integrated MDC peak intensities plus fit (blue dashed line). (b) Momentum-integrated energy-versus-delay photoemission intensity map of Ir(111), recorded with a photon energy of 36.1 eV (23$^{\text{rd}}$ harmonic), and energy-integrated ($E \geq E_{\text{F}}$) intensity transient (black dots) plus fit (white dashed line). Values for the Gaussian FWHM determined from the fits, corresponding to effective experimental resolutions, are indicated.

A. Experimental resolutions

We estimated the effective experimental energy and momentum resolutions from the Fermi-level crossing of the graphene π-band in the graphene/Ir(111) sample. Figure 3(a) shows an E–k photoemission intensity map, which was measured in the vicinity of the K point with a photon energy of 33 eV (21$^{\text{st}}$ harmonic) using probe-only photoemission. Also shown are the momentum distribution curve (MDC) extracted at E_{F} (top panel) and an energy distribution curve (EDC) obtained by the MDC method[56] (right panel), representing the energy distribution of fitted MDC peak areas.

The EDC was fitted with a room-temperature Fermi-Dirac distribution function convoluted with a Gaussian resolution function [Fig. 3(a), right panel]. The resulting Gaussian FWHM, corresponding to the total energy resolution, is (96 ± 4) meV. This value includes a contribution of the photon source and monochromator on the order of 90 meV. The contribution of the electron spectrometer including space-charge broadening is estimated to be 30 meV. Over the entire usable spectral range of ≈24–46 eV, the effective energy resolution varied between 80 and 135 meV, where the photon-energy dependence of the grating resolution at fixed slit widths makes the dominant contribution.

The Gaussian FWHM determined from the momentum distribution curve at E_{F} is (0.096 ± 0.003) Å^{-1} [Fig. 3(a), top panel]. After subtracting the intrinsic π-band momentum width of 0.031 Å^{-1},[57,58] the remaining effective momentum resolution is (0.091 ± 0.003) Å^{-1}. We attribute the deterioration with respect to the nominal momentum resolution to less than optimal sample quality, electronic noise, and timing jitter in the position measurement. With varying probe photon energy, no noticeable changes of the momentum resolution were detected.

To estimate the temporal cross-correlation between pump and probe pulses, we performed pump-probe photoemission measurements on pristine Ir(111) using pump and probe photon energies of 1.57 eV and 36.1 eV (23$^{\text{rd}}$ harmonic), respectively, and an incident pump fluence of 2.42 mJ/cm^2. Figure 3(b) shows a momentum-integrated E–t_{D} intensity map depicting the transient generation and relaxation of hot electrons above E_{F}. A corresponding intensity transient (black data points), obtained by integrating over energies larger than E_{F}, is overlaid. This signal was fitted with a step function multiplied by an exponential decay and convoluted with a Gaussian function. The resulting Gaussian FWHM is (95 ± 5) fs, giving an estimate of the temporal system response function. Based on this value and with a modeled pump pulse duration of (67 ± 5) fs FWHM at the sample position, we estimate the duration of the probe pulse to (67 ± 5) fs FWHM, assuming uncorrelated Gaussian-shaped pulses.

B. Multispectral energy-momentum mapping

The key novel characteristic of our experimental setup is the combination of highly efficient 3D photoemission intensity $I(E, k_x, k_y)$ imaging with a discrete tunability of the probe photon energy, thus making the energy-momentum mapping in trARPES k_z-dependent and 4D. Figure 4 illustrates this experimental advance.

The central panel of Fig. 4 displays two typical XUV spectra as a function of the monochromator energy. The spectrum indicated by the black line gives the calculated photon flux at the sample position. This signal was measured by a calibrated XUV-sensitive Si photodiode behind the exit slit of the monochromator and corrected for beamline transmission including Al-filter attenuation to prevent photocurrent satu-

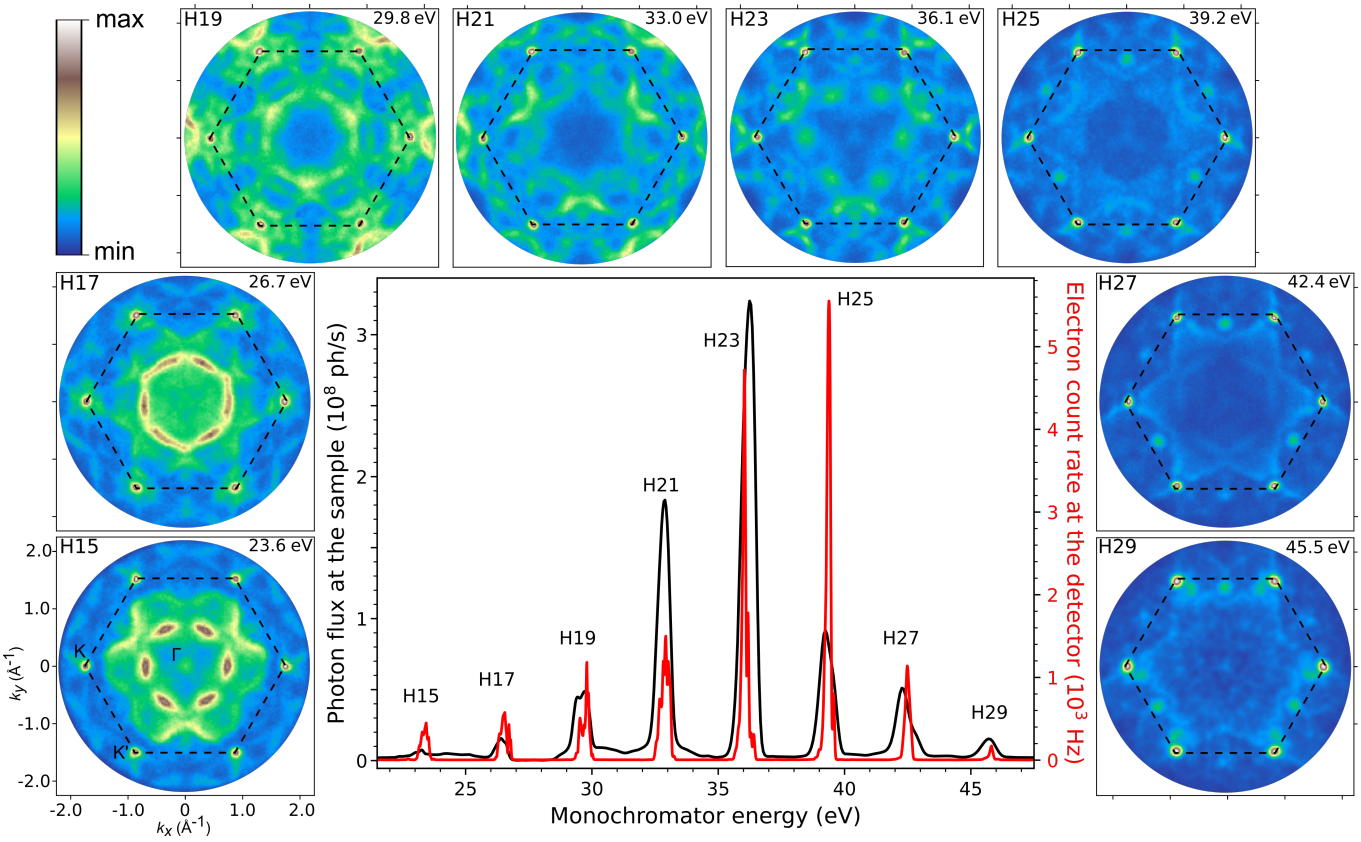

FIG. 4. Multispectral Fermi surface mapping of graphene/Ir(111) using higher-harmonic-generation-based time-of-flight momentum microscopy. Central panel: Higher harmonic spectra as given by photon flux (black line) and electron count rate (red line). Spectra were measured with an XUV-sensitive photodiode behind the exit slit of the monochromator and with the momentum microscope from a graphene-covered Ir(111) sample, respectively. The photon flux at the sample position was calculated accounting for beamline transmission and beam attenuation. For the scans, the slit sizes of the monochromator were adjusted to a monochromator resolution of 150 meV at the 23rd harmonic. Surrounding panels: Full series of Fermi-surface maps taken over the photon-energy tuning range from 23.6 to 45.5 eV (15th to 29th harmonic). The hexagonal Brillouin zone of graphene is indicated.

ration. The second spectrum (red line) represents the electron count rate at the detector, as measured from an electrically biased graphene/Ir(111) sample by the ToF momentum microscope under otherwise typical measurement settings. The practically useable photon-energy tuning range is 23.6–45.5 eV, at a spacing of ≈3.1 eV, corresponding to the odd harmonic orders 15 to 29. The cutoff at ≈48 eV is typical for Ar gas as a generating medium.[59]

The panels surrounding the XUV spectra in Fig. 4 show Fermi surface maps taken from graphene/Ir(111) with all eight harmonics. These 2D intensity maps are extracted from the full 3D data cubes that were originally measured. The data acquisition times varied from 2 to 12 h. The multispectral Fermi surface maps reflect a superposition of the point-like 2D Fermi surface of graphene (centered at the corners of the indicated hexagonal graphene BZ) and the complex multi-sheet 3D Fermi surface of Ir(111). There is no photon energy-dependent change in the shape of the graphene Fermi points, whereas the variation in the shape of the Ir 5*d* intensity pattern, i.e., k_z dispersion, is pronounced. Another observation is that the relative contribution of the Ir 5*d* signal to the total photoemission intensity at E_F is continuously suppressed upon increasing the photon energy from 23.6 eV to 45.5 eV. We attribute this effect to a decrease in the electron escape depth upon approaching the minimum of the universal curve of the inelastic mean free path around a kinetic energy of ≈50 eV:[60] With increasing surface sensitivity, less photoemission signal is obtained from Ir(111), which is covered by a graphene monolayer.

Under the assumption of free-electron-like final states within the direct-transition model of ARPES, constant-energy maps, such as the ones displayed in Fig. 4, map onto a spherical surface in 3D momentum space. The kinematic equation relating the surface-perpendicular momentum component to the other measurement parameters is:[5]

$$k_z = \sqrt{\frac{2m^*}{\hbar^2}\left[(E-E_F)+h\nu+V_0^*\right]-\left(k_x^2+k_y^2\right)}, \qquad (1)$$

where $h\nu$ is the photon energy and m^* and V_0^* are the effective electron mass and inner potential (referenced to E_F) of the nearly-free-electron final-state parabola, respectively. The empirical parameters for Ir(111) are $m^* = 1.07\,m_e$ and $V_0^* = 10$ eV.[61] Using equation (1) and exploiting point symmetry about the center of the BZ (Γ point), a tomogram of

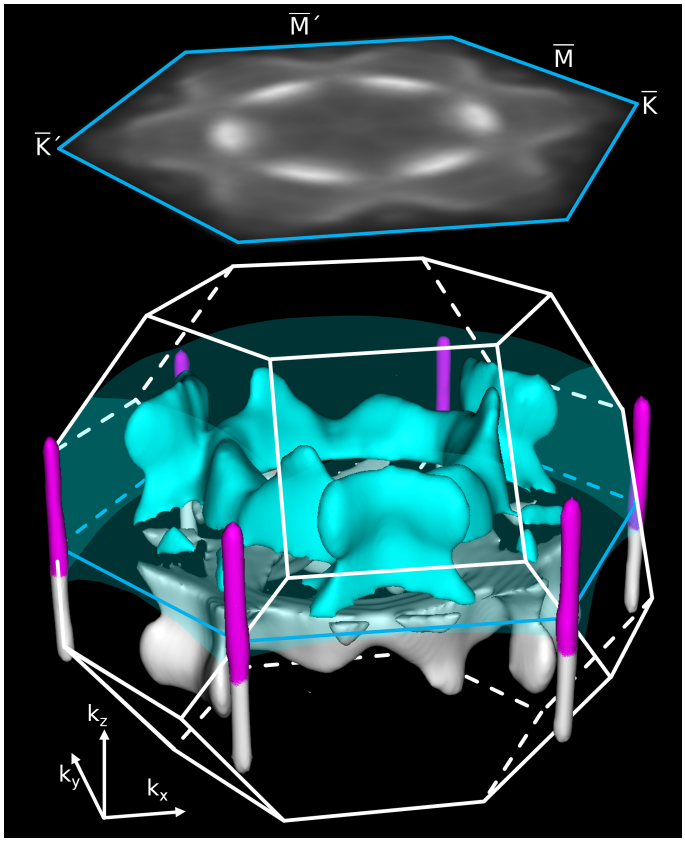

FIG. 5. Lower part: 3D Fermi surface tomogram of graphene/Ir(111), as reconstructed from the Fermi surface maps shown in Fig. 4. The 2D and 3D Brillouin zones of graphene and Ir(111) are indicated by blue and white lines, respectively. Fermi-surface sheets obtained from originally measured data are highlighted by pink and cyan color for graphene and Ir(111), respectively. Corresponding Fermi surface sheets obtained by point reflection about the Γ-point are shown in gray. Top part: Interpolated Fermi surface map through Γ.

the 3D Fermi surface can be reconstructed from the stack of Fermi surface maps shown in Fig. 4.

Figure 5 displays the reconstructed portion of the 3D Fermi surface for graphene/Ir(111). Three sets of isosurfaces can be identified: the non-k_z-dispersive graphene Fermi rods centered at the corners of the hexagonal graphene BZ as well as an inner hexagon-shaped Fermi surface sheet and an outer star-shaped Fermi surface sheet derived from Ir 5*d* bulk states. The reconstructed Ir 5*d* Fermi surface sheets are in good agreement with a 3D Fermi surface tomogram obtained from pristine Ir(111) by soft x-ray momentum microscopy.[61] The available photon-energy range translates into a finite k_z probing interval of $\Delta k_z = 0.9\,\text{Å}^{-1}$, smaller than the characteristic k_z dimension ($\overline{\Gamma L} = 1.42\,\text{Å}^{-1}$) of the fcc BZ of Ir(111). Thus, our tomographic data cover ≈39% of the BZ volume. For crystalline materials with smaller k_z dimensions, particularly layered 3D electron materials,[9,10,17,34] larger portions of the bulk BZ or entire bulk BZs can be scanned. Similarly, for layers of 3D molecules,[62] 3D orbital momentum tomograms can be recorded.

IV. CONCLUSIONS

In conclusion, by combining a 790-nm-driven kHz-repetition-rate HHG source with a plane-grating monochromator and a high-detection-efficiency ToF momentum microscope, we have realized an experimental setup for probe photon energy-dependent time-resolved XUV-ARPES with good data collection efficiency and sub-100-fs time resolution. The photon energy tuning range is ≈24–46 eV, sufficient to map band structures and Fermi surfaces as well as molecular orbital densities over a k_z interval of ≈1 Å^{-1}. The system thus specifically enables k_z-selective probing of ultrafast electronic structure dynamics in 3D materials as well as ultrafast 3D orbital tomography of molecular layers.[32,63] Moreover, the setup complements time-resolved momentum microscopy in the XUV to soft x-ray regime at the FEL FLASH, for which the same ToF momentum microscope is used.[21] The two complementary probe photon sources particularly enable a unique merging of trARPES with time-resolved x-ray photoelectron spectroscopy[64–66] and diffraction[67] for combined investigations of ultrafast electronic, chemical, and geometric structure dynamics.

ACKNOWLEDGMENTS

The work was supported by the Deutsche Forschungsgemeinschaft (DFG, German Research Foundation) via the Collaborative Research Center (CRC) 925—Project ID 170620586 (project B2). We thank Holger Meyer and Sven Gieschen for support with the instrumentation.

DATA AVAILABILITY STATEMENT

The data that support the findings of this study are available from the corresponding author upon reasonable request.

[1] A. Damascelli, "Probing the electronic structure of complex systems by ARPES," Physica Scripta **T109**, 61 (2004).
[2] B. Lv, T. Qian, and H. Ding, "Angle-resolved photoemission spectroscopy and its application to topological materials," Nature Reviews Physics **1**, 609–626 (2019).
[3] P. D. C. King, S. Picozzi, R. G. Egdell, and G. Panaccione, "Angle, spin, and depth resolved photoelectron spectroscopy on quantum materials," Chemical Reviews **121**, 2816–2856 (2021), pMID: 33346644, https://doi.org/10.1021/acs.chemrev.0c00616.
[4] J. A. Sobota, Y. He, and Z.-X. Shen, "Angle-resolved photoemission studies of quantum materials," Rev. Mod. Phys. **93**, 025006 (2021).
[5] T. C. Chiang, J. A. Knapp, M. Aono, and D. E. Eastman, "Angle-resolved photoemission, valence-band dispersions $e(\vec{k})$, and electron and hole lifetimes for gaas," Phys. Rev. B **21**, 3513–3522 (1980).
[6] K. Medjanik, O. Fedchenko, S. Chernov, D. Kutnyakhov, M. Ellguth, A. Oelsner, B. Schönhense, T. R. F. Peixoto, P. Lutz, C.-H. Min, F. Reinert, S. Däster, Y. Acremann, J. Viefhaus, W. Wurth, H. J. Elmers, and G. Schönhense, "Direct 3d mapping of the fermi surface and fermi velocity," Nature Materials **16**, 615–621 (2017).
[7] S. Hüfner, R. Claessen, F. Reinert, T. Straub, V. Strocov, and P. Steiner, "Photoemission spectroscopy in metals:: band structure-fermi surface–spectral function," Journal of Electron Spectroscopy and Related Phenomena **100**, 191–213 (1999).

[8] T. Valla, A. V. Fedorov, P. D. Johnson, and S. L. Hulbert, "Many-body effects in angle-resolved photoemission: Quasiparticle energy and lifetime of a mo(110) surface state," Phys. Rev. Lett. **83**, 2085–2088 (1999).

[9] E. E. Krasovskii, K. Rossnagel, A. Fedorov, W. Schattke, and L. Kipp, "Determination of the hole lifetime from photoemission: Ti 3*d* states in tite$_2$," Phys. Rev. Lett. **98**, 217604 (2007).

[10] M. D. Watson, O. J. Clark, F. Mazzola, I. Marković, V. Sunko, T. K. Kim, K. Rossnagel, and P. D. C. King, "Orbital- and k_z-selective hybridization of se 4*p* and ti 3*d* states in the charge density wave phase of tise$_2$," Phys. Rev. Lett. **122**, 076404 (2019).

[11] P. Puschnig, S. Berkebile, A. J. Fleming, G. Koller, K. Emtsev, T. Seyller, J. D. Riley, C. Ambrosch-Draxl, F. P. Netzer, and M. G. Ramsey, "Reconstruction of molecular orbital densities from photoemission data," Science **326**, 702–706 (2009), https://www.science.org/doi/pdf/10.1126/science.1176105.

[12] M. Graus, C. Metzger, M. Grimm, P. Nigge, V. Feyer, A. Schöll, and F. Reinert, "Three-dimensional tomographic imaging of molecular orbitals by photoelectron momentum microscopy," The European Physical Journal B **92**, 80 (2019).

[13] B. Wannberg, "Electron optics development for photo-electron spectrometers," Nuclear Instruments and Methods in Physics Research Section A: Accelerators, Spectrometers, Detectors and Associated Equipment **601**, 182–194 (2009), special issue in honour of Prof. Kai Siegbahn.

[14] M. Kotsugi, W. Kuch, F. Offi, L. I. Chelaru, and J. Kirschner, "Microspectroscopic two-dimensional fermi surface mapping using a photoelectron emission microscope," Review of Scientific Instruments **74**, 2754–2758 (2003), https://doi.org/10.1063/1.1569404.

[15] G. Schönhense, K. Medjanik, and H.-J. Elmers, "Space-, time- and spin-resolved photoemission," Journal of Electron Spectroscopy and Related Phenomena **200**, 94 – 118 (2015), special Anniversary Issue: Volume 200.

[16] S. Babenkov, K. Medjanik, D. Vasilyev, S. Chernov, C. Schlueter, A. Gloskovskii, Y. Matveyev, W. Drube, B. Schönhense, K. Rossnagel, H.-J. Elmers, and G. Schönhense, "High-accuracy bulk electronic bandmapping with eliminated diffraction effects using hard x-ray photoelectron momentum microscopy," Communications Physics **2**, 107 (2019).

[17] K. Rossnagel, L. Kipp, M. Skibowski, C. Solterbeck, T. Strasser, W. Schattke, D. Voß, P. Krüger, A. Mazur, and J. Pollmann, "Three-dimensional fermi surface determination by angle-resolved photoelectron spectroscopy," Phys. Rev. B **63**, 125104 (2001).

[18] M. B. Nielsen, Z. Li, S. Lizzit, A. Goldoni, and P. Hofmann, "Bulk fermi surface mapping with high-energy angle-resolved photoemission," Journal of Physics: Condensed Matter **15**, 6919–6930 (2003).

[19] V. N. Strocov, M. Kobayashi, X. Wang, L. L. Lev, J. Krempasky, V. V. Rogalev, T. Schmitt, C. Cancellieri, and M. L. Reinle-Schmitt, "Soft-x-ray arpes at the swiss light source: From 3d materials to buried interfaces and impurities," Synchrotron Radiation News **27**, 31–40 (2014), https://doi.org/10.1080/08940886.2014.889550.

[20] S. Moser, "An experimentalist's guide to the matrix element in angle resolved photoemission," Journal of Electron Spectroscopy and Related Phenomena **214**, 29–52 (2017).

[21] D. Kutnyakhov, R. P. Xian, M. Dendzik, M. Heber, F. Pressacco, S. Y. Agustsson, L. Wenthaus, H. Meyer, S. Gieschen, G. Mercurio, A. Benz, K. Bühlman, S. Däster, R. Gort, D. Curcio, K. Volckaert, M. Bianchi, C. Sanders, J. A. Miwa, S. Ulstrup, A. Oelsner, C. Tusche, Y.-J. Chen, D. Vasilyev, K. Medjanik, G. Brenner, S. Dziarzhytski, H. Redlin, B. Manschwetus, S. Dong, J. Hauer, L. Rettig, F. Diekmann, K. Rossnagel, J. Demsar, H.-J. Elmers, P. Hofmann, R. Ernstorfer, G. Schönhense, Y. Acremann, and W. Wurth, "Time- and momentum-resolved photoemission studies using time-of-flight momentum microscopy at a free-electron laser," Review of Scientific Instruments **91**, 013109 (2020), https://doi.org/10.1063/1.5118777.

[22] J. Maklar, S. Dong, S. Beaulieu, T. Pincelli, M. Dendzik, Y. W. Windsor, R. P. Xian, M. Wolf, R. Ernstorfer, and L. Rettig, "A quantitative comparison of time-of-flight momentum microscopes and hemispherical analyzers for time- and angle-resolved photoemission spectroscopy experiments," Review of Scientific Instruments **91**, 123112 (2020), https://doi.org/10.1063/5.0024493.

[23] L. Perfetti, P. A. Loukakos, M. Lisowski, U. Bovensiepen, H. Berger, S. Biermann, P. S. Cornaglia, A. Georges, and M. Wolf, "Time evolution of the electronic structure of $1t-\text{tas}_2$ through the insulator-metal transition," Phys. Rev. Lett. **97**, 067402 (2006).

[24] F. Schmitt, P. S. Kirchmann, U. Bovensiepen, R. G. Moore, L. Rettig, M. Krenz, J.-H. Chu, N. Ru, L. Perfetti, D. H. Lu, M. Wolf, I. R. Fisher, and Z.-X. Shen, "Transient electronic structure and melting of a charge density wave in tbte₃," Science **321**, 1649–1652 (2008), https://www.science.org/doi/pdf/10.1126/science.1160778.

[25] T. Rohwer, S. Hellmann, M. Wiesenmayer, C. Sohrt, A. Stange, B. Slomski, A. Carr, Y. Liu, L. M. Avila, M. Kalläne, S. Mathias, L. Kipp, K. Rossnagel, and M. Bauer, "Collapse of long-range charge order tracked by time-resolved photoemission at high momenta," Nature **471**, 490–493 (2011).

[26] C. L. Smallwood, J. P. Hinton, C. Jozwiak, W. Zhang, J. D. Koralek, H. Eisaki, D.-H. Lee, J. Orenstein, and A. Lanzara, "Tracking cooper pairs in a cuprate superconductor by ultrafast angle-resolved photoemission," Science **336**, 1137–1139 (2012), https://www.science.org/doi/pdf/10.1126/science.1217423.

[27] I. Gierz, J. C. Petersen, M. Mitrano, C. Cacho, I. C. E. Turcu, E. Springate, A. Stöhr, A. Köhler, U. Starke, and A. Cavalleri, "Snapshots of non-equilibrium dirac carrier distributions in graphene," Nature Materials **12**, 1119–1124 (2013).

[28] Y. H. Wang, H. Steinberg, P. Jarillo-Herrero, and N. Gedik, "Observation of floquet-bloch states on the surface of a topological insulator," Science **342**, 453–457 (2013), https://www.science.org/doi/pdf/10.1126/science.1239834.

[29] F. Mahmood, C.-K. Chan, Z. Alpichshev, D. Gardner, Y. Lee, P. A. Lee, and N. Gedik, "Selective scattering between floquet–bloch and volkov states in a topological insulator," Nature Physics **12**, 306–310 (2016).

[30] C. W. Nicholson, A. Lücke, W. G. Schmidt, M. Puppin, L. Rettig, R. Ernstorfer, and M. Wolf, "Beyond the molecular movie: Dynamics of bands and bonds during a photoinduced phase transition," Science **362**, 821–825 (2018), https://www.science.org/doi/pdf/10.1126/science.aar4183.

[31] M. X. Na, A. K. Mills, F. Boschini, M. Michiardi, B. Nosarzewski, R. P. Day, E. Razzoli, A. Sheyerman, M. Schneider, G. Levy, S. Zhdanovich, T. P. Devereaux, A. F. Kemper, D. J. Jones, and A. Damascelli, "Direct determination of mode-projected electron-phonon coupling in the time domain," Science **366**, 1231–1236 (2019), https://www.science.org/doi/pdf/10.1126/science.aaw1662.

[32] R. Wallauer, M. Raths, K. Stallberg, L. Münster, D. Brandstetter, X. Yang, J. Güdde, P. Puschnig, S. Soubatch, C. Kumpf, F. C. Bocquet, F. S. Tautz, and U. Höfer, "Tracing orbital images on ultrafast time scales," Science (2021), 10.1126/science.abf3286.

[33] A. Gauthier, J. A. Sobota, N. Gauthier, K.-J. Xu, H. Pfau, C. R. Rotundu, Z.-X. Shen, and P. S. Kirchmann, "Tuning time and energy resolution in time-resolved photoemission spectroscopy with nonlinear crystals," Journal of Applied Physics **128**, 093101 (2020), https://doi.org/10.1063/5.0018834.

[34] C. Bao, H. Zhong, S. Zhou, R. Feng, Y. Wang, and S. Zhou, "Ultrafast time- and angle-resolved photoemission spectroscopy with widely tunable probe photon energy of 5.3–7.0 ev for investigating dynamics of three-dimensional materials," Review of Scientific Instruments **93**, 013902 (2022), https://doi.org/10.1063/5.0070004.

[35] G. L. Dakovski, Y. Li, T. Durakiewicz, and G. Rodriguez, "Tunable ultrafast extreme ultraviolet source for time- and angle-resolved photoemission spectroscopy," Review of Scientific Instruments **81**, 073108 (2010), https://doi.org/10.1063/1.3460267.

[36] B. Frietsch, R. Carley, K. Döbrich, C. Gahl, M. Teichmann, O. Schwarzkopf, P. Wernet, and M. Weinelt, "A high-order harmonic generation apparatus for time- and angle-resolved photoelectron spectroscopy," Review of Scientific Instruments **84**, 075106 (2013), https://doi.org/10.1063/1.4812992.

[37] S. Eich, A. Stange, A. Carr, J. Urbancic, T. Popmintchev, M. Wiesenmayer, K. Jansen, A. Ruffing, S. Jakobs, T. Rohwer, S. Hellmann, C. Chen, P. Matyba, L. Kipp, K. Rossnagel, M. Bauer, M. Murnane, H. Kapteyn, S. Mathias, and M. Aeschlimann, "Time- and angle-resolved photoemission spectroscopy with optimized high-harmonic pulses using frequency-doubled ti:sapphire lasers," Journal of Electron Spectroscopy and Related Phenomena **195**, 231–236 (2014).

[38] F. Cilento, A. Crepaldi, G. Manzoni, A. Sterzi, M. Zacchigna, P. Bugnon, H. Berger, and F. Parmigiani, "Advancing non-equilibrium arpes experiments by a 9.3ev coherent ultrafast photon source," Journal of Electron Spectroscopy and Related Phenomena **207**, 7–13 (2016).

[39] G. Rohde, A. Hendel, A. Stange, K. Hanff, L.-P. Oloff, L. X. Yang, K. Rossnagel, and M. Bauer, "Time-resolved arpes with sub-15 fs temporal and near fourier-limited spectral resolution," Review of Scientific Instruments **87**, 103102 (2016), https://doi.org/10.1063/1.4963668.

[40] C. Corder, P. Zhao, J. Bakalis, X. Li, M. D. Kershis, A. R. Muraca, M. G. White, and T. K. Allison, "Ultrafast extreme ultraviolet photoemission without space charge," Structural Dynamics **5**, 054301 (2018), https://doi.org/10.1063/1.5045578.

[41] M. Puppin, Y. Deng, C. W. Nicholson, J. Feldl, N. B. M. Schröter, H. Vita, P. S. Kirchmann, C. Monney, L. Rettig, M. Wolf, and R. Ernstorfer, "Time- and angle-resolved photoemission spectroscopy of solids in the extreme ultraviolet at 500 khz repetition rate," Review of Scientific Instruments **90**, 023104 (2019), https://doi.org/10.1063/1.5081938.

[42] J. H. Buss, H. Wang, Y. Xu, J. Maklar, F. Joucken, L. Zeng, S. Stoll, C. Jozwiak, J. Pepper, Y.-D. Chuang, J. D. Denlinger, Z. Hussain, A. Lanzara, and R. A. Kaindl, "A setup for extreme-ultraviolet ultrafast angle-resolved photoelectron spectroscopy at 50-khz repetition rate," Review of Scientific Instruments **90**, 023105 (2019), https://doi.org/10.1063/1.5079677.

[43] E. J. Sie, T. Rohwer, C. Lee, and N. Gedik, "Time-resolved XUV arpes with tunable 24-33 ev laser pulses at 30 mev resolution," Nature Communications **10**, 3535– (2019).

[44] A. K. Mills, S. Zhdanovich, M. X. Na, F. Boschini, E. Razzoli, M. Michiardi, A. Sheyerman, M. Schneider, T. J. Hammond, V. Süss, C. Felser, A. Damascelli, and D. J. Jones, "Cavity-enhanced high harmonic generation for extreme ultraviolet time- and angle-resolved photoemission spectroscopy," Review of Scientific Instruments **90**, 083001 (2019), https://doi.org/10.1063/1.5090507.

[45] Y. Liu, J. E. Beetar, M. M. Hosen, G. Dhakal, C. Sims, F. Kabir, M. B. Etienne, K. Dimitri, S. Regmi, Y. Liu, A. K. Pathak, D. Kaczorowski, M. Neupane, and M. Chini, "Extreme ultraviolet time- and angle-resolved photoemission setup with 21.5 mev resolution using high-order harmonic generation from a turn-key yb:kgw amplifier," Review of Scientific Instruments **91**, 013102 (2020), https://doi.org/10.1063/1.5121425.

[46] R. Cucini, T. Pincelli, G. Panaccione, D. Kopic, F. Frassetto, P. Miotti, G. M. Pierantozzi, S. Peli, A. Fondacaro, A. De Luisa, A. De Vita, P. Carrara, D. Krizmancic, D. T. Payne, F. Salvador, A. Sterzi, L. Poletto, F. Parmigiani, G. Rossi, and F. Cilento, "Coherent narrowband light source for ultrafast photoelectron spectroscopy in the 17–31 ev photon energy range," Structural Dynamics **7**, 014303 (2020), https://doi.org/10.1063/1.5131216.

[47] C. Lee, T. Rohwer, E. J. Sie, A. Zong, E. Baldini, J. Straquadine, P. Walmsley, D. Gardner, Y. S. Lee, I. R. Fisher, and N. Gedik, "High resolution time- and angle-resolved photoemission spectroscopy with 11 ev laser pulses," Review of Scientific Instruments **91**, 043102 (2020), https://doi.org/10.1063/1.5139556.

[48] M. Keunecke, C. Möller, D. Schmitt, H. Nolte, G. S. M. Jansen, M. Reutzel, M. Gutberlet, G. Halasi, D. Steil, S. Steil, and S. Mathias, "Time-resolved momentum microscopy with a 1 mhz high-harmonic extreme ultraviolet beamline," Review of Scientific Instruments **91**, 063905 (2020), https://doi.org/10.1063/5.0006531.

[49] S. Peli, D. Puntel, D. Kopic, B. Sockol, F. Parmigiani, and F. Cilento, "Time-resolved vuv arpes at 10.8 ev photon energy and mhz repetition rate," Journal of Electron Spectroscopy and Related Phenomena **243**, 146978 (2020).

[50] Q. Guo, M. Dendzik, A. Grubišić-Čabo, M. H. Berntsen, C. Li, W. Chen, B. Matta, U. Starke, B. Hessmo, J. Weissenrieder, and O. Tjernberg, "A narrow bandwidth extreme ultra-violet light source for time- and angle-resolved photoemission spectroscopy," (2022), arXiv:2201.12456 [cond-mat.str-el].

[51] N. C. Gerken, *XUV Multiphoton Excitation and Charged State Dynamics in Small Quantum Systems* (Verlag Dr. Hut, 2014).

[52] N. Gerken, S. Klumpp, A. A. Sorokin, K. Tiedtke, M. Richter, V. Bürk, K. Mertens, P. Juranić, and M. Martins, "Time-dependent multiphoton ionization of xenon in the soft-x-ray regime," Phys. Rev. Lett. **112**, 213002 (2014).

[53] R. P. Xian, Y. Acremann, S. Y. Agustsson, M. Dendzik, K. Bühlmann, D. Curcio, D. Kutnyakhov, F. Pressacco, M. Heber, S. Dong, T. Pincelli, J. Demsar, W. Wurth, P. Hofmann, M. Wolf, M. Scheidgen, L. Rettig, and R. Ernstorfer, "An open-source, end-to-end workflow for multidimensional photoemission spectroscopy," Scientific Data **7**, 442 (2020).

[54] C. Tusche, P. Goslawski, D. Kutnyakhov, M. Ellguth, K. Medjanik, H. J. Elmers, S. Chernov, R. Wallauer, D. Engel, A. Jankowiak, and G. Schönhense, "Multi-mhz time-of-flight electronic bandstructure imaging of graphene on ir(111)," Applied Physics Letters **108**, 261602 (2016), https://doi.org/10.1063/1.4955015.

[55] A. T. N'Diaye, J. Coraux, T. N. Plasa, C. Busse, and T. Michely, "Structure of epitaxial graphene on ir(111)," New Journal of Physics **10**, 043033 (2008).

[56] S. Ulstrup, J. C. Johannsen, M. Grioni, and P. Hofmann, "Extracting the temperature of hot carriers in time- and angle-resolved photoemission," Review of Scientific Instruments **85**, 013907 (2014), https://doi.org/10.1063/1.4863322.

[57] M. Kralj, I. Pletikosić, M. Petrović, P. Pervan, M. Milun, A. T. N'Diaye, C. Busse, T. Michely, J. Fujii, and I. Vobornik, "Graphene on ir(111) characterized by angle-resolved photoemission," Phys. Rev. B **84**, 075427 (2011).

[58] J. C. Johannsen, S. Ulstrup, M. Bianchi, R. Hatch, D. Guan, F. Mazzola, L. Hornekær, F. Fromm, C. Raidel, T. Seyller, and P. Hofmann, "Electron–phonon coupling in quasi-free-standing graphene," Journal of Physics: Condensed Matter **25**, 094001 (2013).

[59] J. L. Krause, K. J. Schafer, and K. C. Kulander, "High-order harmonic generation from atoms and ions in the high intensity regime," Phys. Rev. Lett. **68**, 3535–3538 (1992).

[60] S. Tanuma, C. J. Powell, and D. R. Penn, "Calculations of electron inelastic mean free paths. ix. data for 41 elemental solids over the 50 ev to 30 kev range," Surface and Interface Analysis **43**, 689–713 (2011), https://onlinelibrary.wiley.com/doi/pdf/10.1002/sia.3522.

[61] H. J. Elmers, D. Kutnyakhov, S. V. Chernov, K. Medjanik, O. Fedchenko, A. Zaporozhchenko-Zymakova, M. Ellguth, C. Tusche, J. Viefhaus, and G. Schönhense, "Hosting of surface states in spin–orbit induced projected bulk band gaps of w(1 1 0) and ir(1 1 1)," Journal of Physics: Condensed Matter **29**, 255001 (2017).

[62] N. Haag, D. Lüftner, F. Haag, J. Seidel, L. L. Kelly, G. Zamborlini, M. Jugovac, V. Feyer, M. Aeschlimann, P. Puschnig, M. Cinchetti, and B. Stadtmüller, "Signatures of an atomic crystal in the band structure of a c_{60} thin film," Phys. Rev. B **101**, 165422 (2020).

[63] M. Scholz, K. Baumgärtner, C. Metzger, D. Kutnyakhov, M. Heber, C. H. Min, T. R. F. Peixoto, M. Reiser, C. Kim, W. Lu, R. Shayduk, W. M. Izquierdo, G. Brenner, F. Roth, F. Pressacco, A. Schöll, S. Molodtsov, W. Wurth, F. Reinert, and A. Madsen, "Ultrafast molecular orbital imaging of a pentacene thin film using a free electron laser," (2019), arXiv:1907.10434 [cond-mat.mes-hall].

[64] S. Hellmann, M. Beye, C. Sohrt, T. Rohwer, F. Sorgenfrei, H. Redlin, M. Kalläne, M. Marczynski-Bühlow, F. Hennies, M. Bauer, A. Föhlisch, L. Kipp, W. Wurth, and K. Rossnagel, "Ultrafast melting of a charge-density wave in the mott insulator $1t-tas_2$," Phys. Rev. Lett. **105**, 187401 (2010).

[65] M. Dendzik, R. P. Xian, E. Perfetto, D. Sangalli, D. Kutnyakhov, S. Dong, S. Beaulieu, T. Pincelli, F. Pressacco, D. Curcio, S. Y. Agustsson, M. Heber, J. Hauer, W. Wurth, G. Brenner, Y. Acremann, P. Hofmann, M. Wolf, A. Marini, G. Stefanucci, L. Rettig, and R. Ernstorfer, "Observation of an excitonic mott transition through ultrafast core-cum-conduction photoemission spectroscopy," Phys. Rev. Lett. **125**, 096401 (2020).

[66] F. Pressacco, D. Sangalli, V. Uhlíř, D. Kutnyakhov, J. A. Arregi, S. Y. Agustsson, G. Brenner, H. Redlin, M. Heber, D. Vasilyev, J. Demsar, G. Schönhense, M. Gatti, A. Marini, W. Wurth, and F. Sirotti, "Subpicosecond metamagnetic phase transition in FeRh driven by non-equilibrium electron dynamics," Nature Communications **12**, 5088 (2021).

[67] D. Curcio, S. Pakdel, K. Volckaert, J. A. Miwa, S. Ulstrup, N. Lanatà, M. Bianchi, D. Kutnyakhov, F. Pressacco, G. Brenner, S. Dziarzhytski, H. Redlin, S. Y. Agustsson, K. Medjanik, D. Vasilyev, H.-J. Elmers, G. Schönhense, C. Tusche, Y.-J. Chen, F. Speck, T. Seyller, K. Bühlmann, R. Gort, F. Diekmann, K. Rossnagel, Y. Acremann, J. Demsar, W. Wurth, D. Lizzit, L. Bignardi, P. Lacovig, S. Lizzit, C. E. Sanders, and P. Hofmann, "Ultrafast electronic linewidth broadening in the c 1*s* core level of graphene," Phys. Rev. B **104**, L161104 (2021).